

## Threshold Gain Reduction in Tandem Semiconductor Nano-Lasers

Fan, Yuanlong; Zhang, Jing; Shore, K. Alan

### Photonics

DOI:  
[10.3390/photonics11111037](https://doi.org/10.3390/photonics11111037)

Published: 05/11/2024

Publisher's PDF, also known as Version of record

[Cyswllt i'r cyhoeddiad / Link to publication](#)

*Dyfyniad o'r fersiwn a gyhoeddwyd / Citation for published version (APA):*  
Fan, Y., Zhang, J., & Shore, K. A. (2024). Threshold Gain Reduction in Tandem Semiconductor Nano-Lasers. *Photonics*, 11(11), Article 1037. <https://doi.org/10.3390/photonics11111037>

#### Hawliau Cyffredinol / General rights

Copyright and moral rights for the publications made accessible in the public portal are retained by the authors and/or other copyright owners and it is a condition of accessing publications that users recognise and abide by the legal requirements associated with these rights.


- Users may download and print one copy of any publication from the public portal for the purpose of private study or research.
- You may not further distribute the material or use it for any profit-making activity or commercial gain
- You may freely distribute the URL identifying the publication in the public portal ?

#### Take down policy

If you believe that this document breaches copyright please contact us providing details, and we will remove access to the work immediately and investigate your claim.

Article

# Threshold Gain Reduction in Tandem Semiconductor Nano-Lasers

Yuanlong Fan <sup>1,2,\*</sup> , Jing Zhang <sup>1,2</sup> and K. Alan Shore <sup>3</sup> 

<sup>1</sup> Hangzhou Institute of Technology, Xidian University, Hangzhou 311200, China; 23191214791@stu.xidian.edu.cn

<sup>2</sup> School of Optoelectronic Engineering, Xidian University, Xi'an 710071, China

<sup>3</sup> School of Computer Science and Electronic Engineering, Bangor University, Bangor LL57 1UT, UK; k.a.shore@bangor.ac.uk

\* Correspondence: fanyuanlong@xidian.edu.cn

**Abstract:** It is shown that a significant reduction in the threshold gain of electrically pumped semiconductor nano-lasers may be achieved in bridge-connected tandem semiconductor nano-lasers. Optimization of the design is achieved by exploring the impact of bridge length and width on the threshold gain. In addition, a detailed examination is also made of the emission patterns of the structure. It is found that a trade-off emerges between threshold gain and beam quality where multi-lobed far field emission may be associated with the lowest threshold gains.

**Keywords:** threshold gain; semiconductor nano-lasers; coupled nano-lasers

## 1. Introduction

The development of electrically pumped semiconductor nano-lasers has presented considerable technical challenges that have spurred many innovative designs [1–4]. The present authors and their co-workers have offered one approach to the design of electrically pumped nano-lasers [5], which awaits practical realization. In anticipation of the availability of such nano-lasers, work has been undertaken to delineate the dynamical features of these devices both as stand-alone devices [6,7] and as coupled elements of arrays [8,9]. In addition to their provision of novel dynamical behaviors, coupled nano-lasers have potential in regard to mitigating some of the challenges to the practical demonstration of electrically pumped nano-lasers. Such potential has been recognized in recent studies where imaginative structures have been studied in detail [10–12]. The present paper pursues that theme by offering a detailed study of the opportunities for utilizing bridge-waveguide-coupled nano-lasers to affect a significant reduction in threshold gain. The specific approach taken here is to examine how the dimensions of the waveguide bridge affect the operating characteristics of the coupled nano-lasers both in terms of the threshold gain and the optical modes excited in the coupled nano-lasers. Characteristics of uncoupled nano-lasers are presented as a benchmark to compare the influence of the bridge, and then attention is given to the impact of the waveguide bridge.

The paper proceeds by presenting schematic diagrams of the uncoupled and coupled nano-laser structures and outlines the numerical modeling technique utilized in their study. A representative set of results is then presented for both types of structures. These include key results showing how the threshold gain of the coupled nano-lasers may be reduced by suitably adjusting the width and length of the waveguide bridge. A brief conclusion from the work is drawn in the final section.

## 2. Model

The 3D diagram of uncoupled and coupled nano-lasers and the illustrations of its cross-section are shown in Figure 1a–c. The coupled nano-laser is located on an InP substrate. The core of this coupled nano-laser is InGaAs, which is sequentially coated with SiO<sub>2</sub> and silver with thicknesses of  $t_C$ ,  $t_S$ , and  $t_M$ , respectively. The SiO<sub>2</sub> layer prevents the diode



**Citation:** Fan, Y.; Zhang, J.; Shore, K.A. Threshold Gain Reduction in Tandem Semiconductor Nano-Lasers. *Photonics* **2024**, *11*, 1037. <https://doi.org/10.3390/photonics11111037>

Received: 21 October 2024

Revised: 31 October 2024

Accepted: 4 November 2024

Published: 5 November 2024



**Copyright:** © 2024 by the authors. Licensee MDPI, Basel, Switzerland. This article is an open access article distributed under the terms and conditions of the Creative Commons Attribution (CC BY) license (<https://creativecommons.org/licenses/by/4.0/>).

from electrically shorting. Silver is utilized to confine the mode. The length and width of bridge-waveguide-coupled nano-lasers connecting two single lasers are  $l_{\text{bridge}}$  and  $w_{\text{bridge}}$ , respectively, as shown in Figure 1c. The dimensions of each layer for a single laser are shown in Table 1. The structure of the single nano-laser is similar to the nano-laser in [2], which can be electrically pumped except that the  $\text{SiO}_2$  is replaced by  $\alpha\text{-Al}_2\text{O}_3$  in [2]. It should be noted that manufactured devices may deviate from the ideal; for example, there may be sidewall tilts [13]. In addition, surface roughness may be introduced during the manufacturing process. These defects will tend to degrade the performance of coupled nano-lasers. Therefore, it is necessary to design a robust SNL to ensure that it is minimally affected by non-idealities introduced in the manufacturing process.

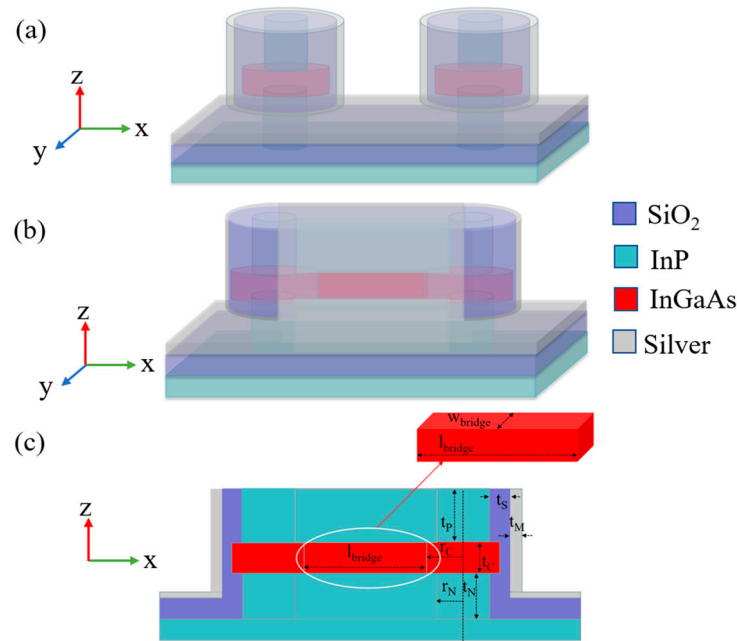


**Figure 1.** The schematic illustration of the uncoupled and coupled nano-laser structures. (a) A 3D schematic of uncoupled nano-lasers. (b) A 3D schematic of coupled nano-lasers. (c) Cross-sectional view of coupled nano-lasers.

**Table 1.** The size of each layer of the coupled nano-laser.

Layer Name	Material	Size
InGaAs Core	InGaAs	$t_C = 300 \text{ nm}$ , $r_C = 350 \text{ nm}$
N Doped Layer	N InP	$t_N = 450 \text{ nm}$ , $r_N = 250 \text{ nm}$
P Doped Layer	P InP	$t_P = 470 \text{ nm}$
Insulating Layer	$\text{SiO}_2$	$t_S = 100 \text{ nm}$
Metal Layer	Ag	$t_M = 30 \text{ nm}$
Bridge	InGaAs	$l_{\text{bridge}} = \text{variable}$ , $w_{\text{bridge}} = \text{variable}$

We calculate the wave vector and electromagnetic field by using the 3D full-wave finite difference time domain (FDTD) method. The mesh size is limited to a fraction of the wavelength. Perfect matched layers (PMLs) are used to surround the lasers to ensure no back-reflections of the light. The quality factor  $Q$  is calculated by (1), where  $k_{\text{real}}$  and  $k_{\text{imag}}$  represent the real and imaginary parts of the wave vector, respectively.

$$Q = \frac{k_{\text{real}}}{2k_{\text{imag}}} \tag{1}$$

Starting from the electric field distribution of the resonant mode inside the cavity structure, we calculate the confinement factor  $\Gamma$  by integrating the electric field intensity

in the active layer. The threshold gain required to emit the laser in the active layer can be derived from the following Formula (2) [5]:

$$g_{th} = \frac{2\pi n_g}{\lambda Q\Gamma} \tag{2}$$

where  $n_g$  is the group refractive index of the active region, and  $\lambda = 1550$  nm is the resonance wavelength. The refractive indices of InP, InGaAs active layer, and SiO<sub>2</sub> are set to 2.63, 3.4, and 1.45 [2,11], respectively. The permittivity of silver is fitted by the Drude–Lorentzian model to experimental values [14]. From (2), it can be seen that the general rules for designing a SNL with a low threshold gain are as follows: (i) to increase the Q factor, which can be achieved by avoiding modal overlap with the metal; and (ii) to maximize the mode confinement in the active region.

### 3. Results

In order to illustrate the effect of the connecting bridge, Figure 2 displays both horizontal and vertical cross-sections of the electric field intensity in, respectively, a stand-alone semiconductor nano-laser, two uncoupled nano-lasers, and bridge-connected tandem nano-lasers, where  $l_{bridge} = 1175$  nm and  $w_{bridge} = 400$  nm. The electric field intensity of the uncoupled lasers does not deviate markedly from that of the stand-alone laser, but the evanescent coupling between the lasers results in a reduction in threshold gain from  $1035\text{ cm}^{-1}$  (Figure 2d) to  $543\text{ cm}^{-1}$  (Figure 2e). However, as intended, the connecting bridge significantly changes the optical field distribution within the compound device, leading to a further reduction in the threshold gain to  $188\text{ cm}^{-1}$  (Figure 2f). Considering the far fields of the devices, Figure 3 includes 3D plots of the far field as well as 2D polar diagrams of the laser emission. The overall beneficial effect of the connecting bridge is made manifest particularly in the 2D polar plots where the number of emission lobes is progressively reduced as one moves from a single nano-laser (Figure 3d) to uncoupled nano-lasers (Figure 3e) and hence to tandem nano-lasers (Figure 3f).

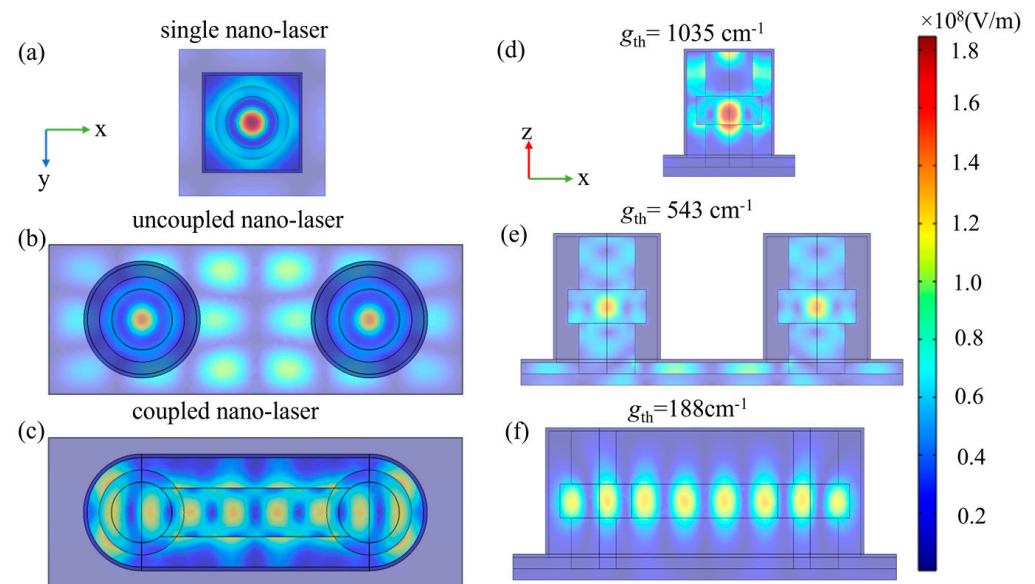


**Figure 2.** Electric field intensity diagram of a single nano-laser, uncoupled nano–laser, and coupled nano–laser. (a–c) Horizontal cross–section. (d–f) Vertical cross–section.

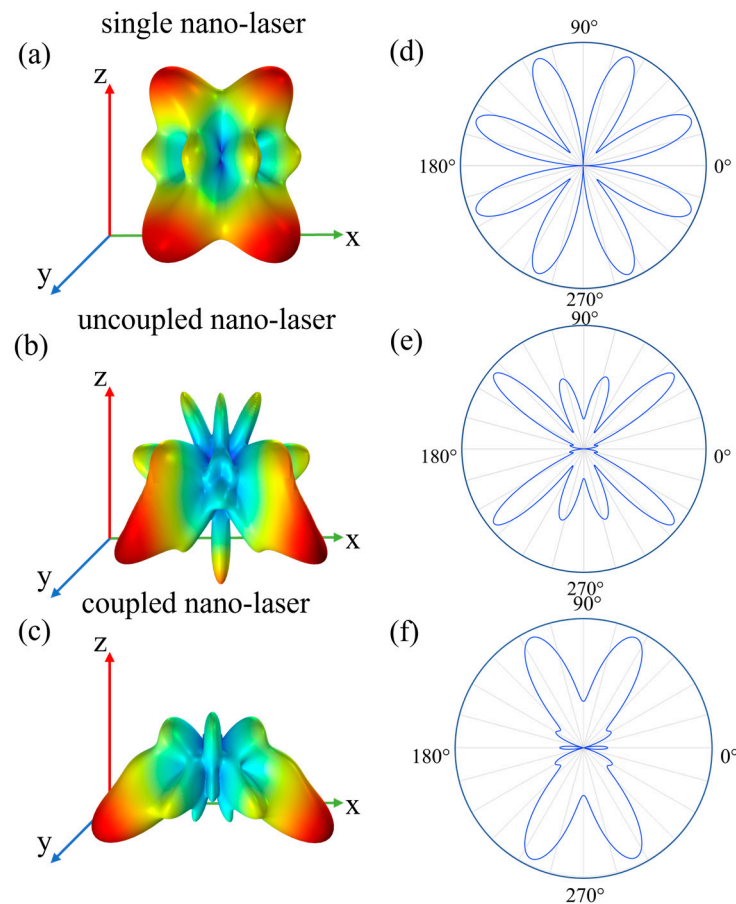


**Figure 3.** Far-field diagram of a single nano-laser, uncoupled nano-laser, and coupled nano-laser. (a–c) A 3D far-field diagram. (d–f) Two-dimensional polar coordinates far-field diagram.

The salient impact of the connecting bridge is captured by Figure 4, which is the product of considerable computational effort. Here, the influence of the bridge width and length on the threshold gain is shown. In essence, the beneficial effect of the bridge is to enhance the coupling between the lasers. A priori, it was expected that the lowest threshold gains would consequently be achieved with relatively wide and short bridges. However, it is seen in Figure 4 that although wider bridges (350 nm to 500 nm) do yield lower threshold gains of order  $200 \text{ cm}^{-1}$ , the bridges are relatively long (900 nm to 1500 nm). A smaller region of low threshold gains is also found for short (300 nm) and narrow (100 nm) bridges, which yield gains of  $130 \text{ cm}^{-1}$  or so. It would appear that the principal factor in determining the gain is the perturbation of the optical field in the device caused by the bridge. The consequences of that are explored in detail below. At this point it is observed that the reduction in threshold gain of several hundred  $\text{cm}^{-1}$  will greatly assist the practical operation of these devices. When consideration is given to the emission patterns of the tandem laser, it is apparent from Figure 5 that there is a trade-off between threshold gain reduction and beam quality. Twin lobes are most prominent in the cases of narrower bridges (150 nm to 250 nm), while quadruple lobes are present in the far field of the widest bridge considered (400 nm).

The consideration of beam quality in the case of varying bridge lengths underlines the challenges for device design as shown in Figure 6. The longest bridge considered (1175 nm) exhibits a two-lobed, well-directed far-field, whereas the shortest bridge (300 nm) delivers emission over a broader angular spread.

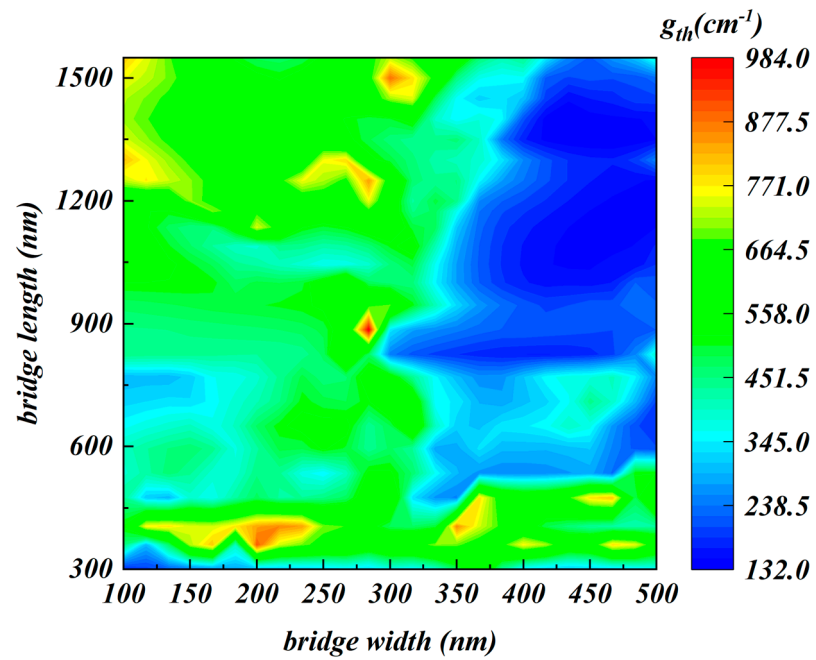


Figure 4. Effect of bridge length and width on threshold gain.

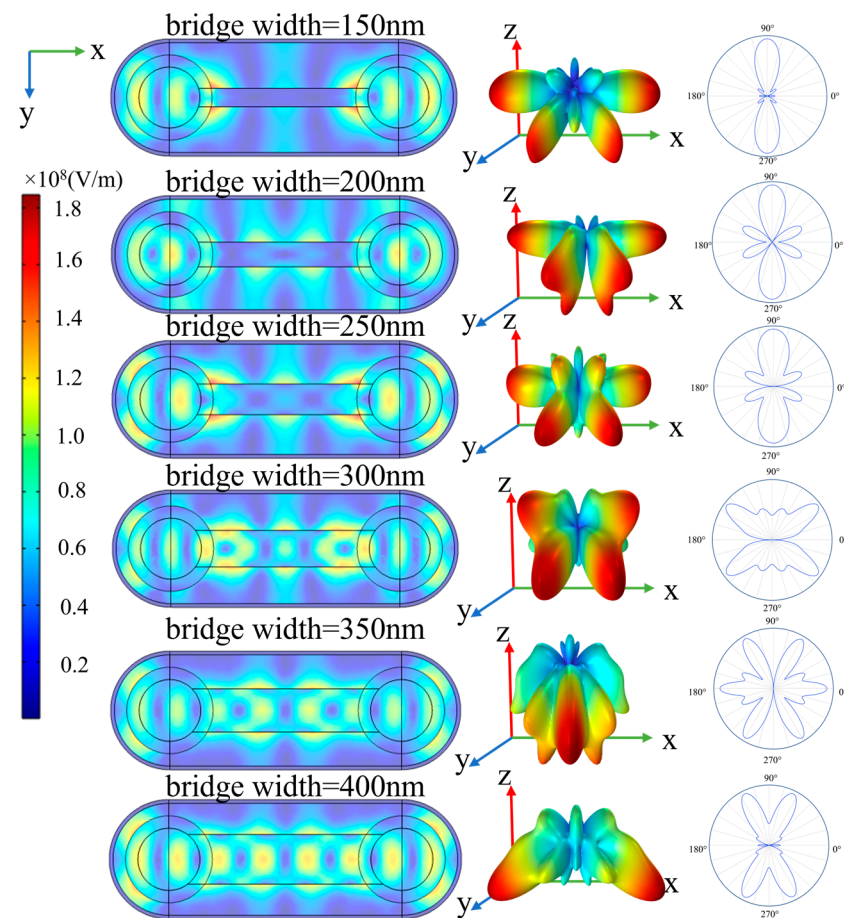
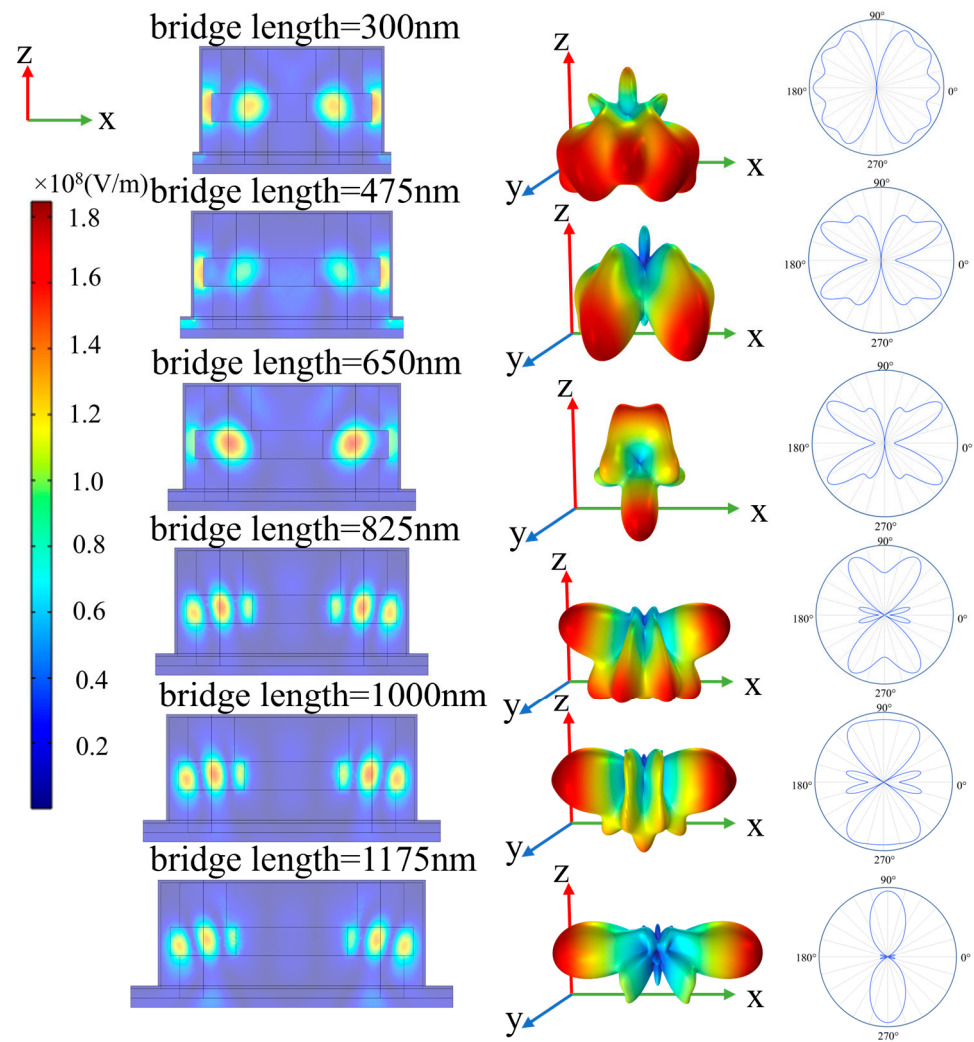


Figure 5. The electric field intensity diagram, 3D far-field distribution, and 2-dimensional polar coordinates far-field diagram of coupled nano-lasers with the increase in the width of the bridge (widths of 150 nm, 200 nm, 250 nm, 300 nm, 350 nm, and 400 nm) when  $l_{\text{bridge}} = 1175$  nm. The first column is the electric field intensity diagram. The second column is a 3D far-field diagram. The third column is a 2-dimensional polar coordinates far-field diagram.



**Figure 6.** The electric field intensity diagram, 3D far-field distribution, and 2-dimensional polar coordinates far-field diagram of coupled nano-lasers with the increase in the length of the bridge (the length of 300 nm, 475 nm, 650 nm, 825 nm, 1000 nm, 1175 nm) when  $w_{\text{bridge}} = 100$  nm. The first column is the electric field intensity diagram. The second column is a 3D far-field diagram. The third column is a 2-dimensional polar coordinate far-field diagram.

**4. Conclusions**

This work has explored the opportunities to achieve reduced threshold gains in tandem semiconductor nano-lasers. A design trade-off is identified by consideration of the beam quality of the laser emission. It is observed that the tandem laser structure studied here may be generalized to a multi-element array where bridge couplers may be used to great effect in reducing the threshold gain.

**Author Contributions:** Conceptualization, K.A.S.; methodology, Y.F. and K.A.S.; software, J.Z.; validation, J.Z. and K.A.S.; formal analysis, Y.F. and K.A.S.; investigation, Y.F. and K.A.S.; resources, Y.F.; data curation, J.Z.; writing—original draft preparation, Y.F. and K.A.S.; writing—review and editing, Y.F., J.Z. and K.A.S.; visualization, J.Z.; supervision, K.A.S.; project administration, Y.F.; funding acquisition, Y.F. All authors have read and agreed to the published version of the manuscript.

**Funding:** This research received no external funding.

**Data Availability Statement:** Data underlying the results presented in this paper are not publicly available at this time but may be obtained from the authors upon reasonable request.

**Conflicts of Interest:** The authors declare no conflicts of interest.

## References

1. Ding, K.; Hill, M.T.; Liu, Z.C.; Yin, L.J.; Van Veldhoven, P.J.; Ning, C.Z. Record Performance of Electrical Injection Sub-Wavelength Metallic-Cavity Semiconductor Lasers at Room Temperature. *Opt. Express* **2013**, *21*, 4728. [[CrossRef](#)] [[PubMed](#)]
2. Gu, Q.; Shane, J.; Vallini, F.; Wingad, B.; Smalley, J.S.T.; Frateschi, N.C.; Fainman, Y. Amorphous Al<sub>2</sub>O<sub>3</sub> Shield for Thermal Management in Electrically Pumped Metallo-Dielectric Nanolasers. *IEEE J. Quantum Electron.* **2014**, *50*, 499–509. [[CrossRef](#)]
3. Li, K.H.; Liu, X.; Wang, Q.; Zhao, S.; Mi, Z. Ultralow-Threshold Electrically Injected AlGaN Nanowire Ultraviolet Lasers on Si Operating at Low Temperature. *Nat. Nanotechnol.* **2015**, *10*, 140–144. [[CrossRef](#)] [[PubMed](#)]
4. Ren, K.; Li, C.; Fang, Z.; Feng, F. Recent Developments of Electrically Pumped Nanolasers. *Laser Photonics Rev.* **2023**, *17*, 2200758. [[CrossRef](#)]
5. Fan, Y.; Shore, K.A. Design of Room Temperature Electrically Pumped Visible Semiconductor Nanolasers. *IEEE J. Quantum Electron.* **2018**, *54*, 2000907. [[CrossRef](#)]
6. Han, H.; Shore, K.A. Dynamical Characteristics of Nano-Lasers Subject to Optical Injection and Phase Conjugate Feedback. *IET Optoelectronics* **2017**, *12*, 25–29. [[CrossRef](#)]
7. Fan, Y.; Hong, Y.; Li, P. Numerical Investigation on Feedback Insensitivity in Semiconductor Nanolasers. *IEEE J. Sel. Top. Quantum Electron.* **2019**, *25*, 1–7. [[CrossRef](#)]
8. Fan, Y.; Shore, K.A.; Shao, X. Dynamics of Electrically Pumped Semiconductor Nano-Laser Arrays. *Photonics*. **2023**, *10*, 1249. [[CrossRef](#)]
9. Fan, Y.; Shi, T.; Zhang, J.; Shore, K.A. Optical Injection Effects in Electrically Pumped Semiconductor Nano-laser Arrays. *Opt. Express* **2024**, *32*, 19361–19371. [[CrossRef](#)] [[PubMed](#)]
10. Deka, S.S.; Pan, S.H.; Gu, Q.; Fainman, Y.; El Amili, A. Coupling in a dual metallo-dielectric nanolaser system. *Opt. Lett.* **2017**, *42*, 4760–4763. [[CrossRef](#)] [[PubMed](#)]
11. Zhang, B.; Zhu, K.; Hao, J.; Wang, B.; Shen, Z.; Hu, H. Design and Numerical Study of Semiconductor Nanolaser with Gaussian-Shaped Metallic Cavity. *IEEE Photonics J.* **2018**, *10*, 4502110. [[CrossRef](#)]
12. Peng, X.; Liu, J.; Kang, Y.; Mao, X.; Yan, W.; Wang, X.; Liu, K.; Xu, R.; Yang, F.; Li, Z. Coupling of Photonic and Plasmonic Modes for Double Nanowire Cavities. *Photonics*. **2023**, *10*, 415. [[CrossRef](#)]
13. Shane, J.; Gu, Q.; Potterton, A.; Fainman, Y. Effect of Undercut Etch on Performance and Fabrication Robustness of Metal-Clad Semiconductor Nanolasers. *IEEE J. Quantum Electron.* **2015**, *51*, 2000109. [[CrossRef](#)]
14. Palik, E.D. *Handbook of Optical Constants of Solids*; Academic Press: London, UK, 1985.

**Disclaimer/Publisher’s Note:** The statements, opinions and data contained in all publications are solely those of the individual author(s) and contributor(s) and not of MDPI and/or the editor(s). MDPI and/or the editor(s) disclaim responsibility for any injury to people or property resulting from any ideas, methods, instructions or products referred to in the content.